INSTITUTE OF PHYSICS PUBLISHING JOURNAL OF PHYSICS: CONDENSED MATTER

J. Phys.: Condens. Matter **14** (2002) R21–R47 PII: S0953-8984(02)17948-3

TOPICAL REVIEW

The standard Gaussian model for block copolymer melts

M W Matsen

Polymer Science Centre, University of Reading, Whiteknights, Reading RG6 6AF, UK

Received 29 August 2001, in final form 12 November 2001
Published 13 December 2001
Online at stacks.iop.org/JPhysCM/14/R21

Abstract

As a result of important advances over the last decade, block copolymer melts have become an excellent model system for studying fundamental phenomena associated with molecular self-assembly. During this time, good quantitative agreement has been achieved between theory and experiment in regards to equilibrium phase behaviour, and with it has emerged a thorough understanding in terms of simple intuitive explanations. The theoretical contributions to this effort are largely attributed to mean-field calculations on a standard Gaussian model. Here, we review this present understanding of block copolymer phase behaviour, the model and its underlying assumptions, the mean-field approximation and its limitations, and the attempts to incorporate fluctuation corrections. Rather than following the traditional rigorous derivations, we present slightly more intuitive and transparent ones in such a way to stress the close connection between the related calculations. In this way, we hope to provide a valuable introduction to block copolymer theory.

1. Introduction

The field of complex liquids attracts tremendous attention, not only because of its rich and intriguing phase behaviour, but also because of its commercial and biological importance. These special liquids encompass a diverse range of molecular systems, typically involving molecules with two ends that interact unfavourably. In order to minimize unfavourable contacts, the molecules tend to self-assemble into ordered microstructures often with very elaborate geometries. By cleverly manipulating this tendency, researchers have created a large host of important applications. Of course, biology has taken advantage of such mechanisms from the very beginning of life. In order to study the phenomena associated with molecular self-assembly, researchers have focused much of their attention on model systems referred to as lyotropic liquid crystals, often involving simple aqueous solutions of either surfactant or lipid molecules [1]. However, more recently, it has become apparent that block copolymer melts, in many ways, provide a superior system for such studies [2].

A polymer is any molecule constructed by linking together chemical units or monomers to form a long-chain molecule. The molecule is called a homopolymer if all the monomers are identical, whereas it is called a copolymer if it involves two or more chemically distinct monomers. If in the latter case the like monomers are grouped together in long sequences (i.e. blocks), the molecule is termed a block copolymer. There exists an endless variety of block copolymer architectures, which can be studied in either the pure form or as blends. Naturally, research begins with the simplest model system, just as the study of atomic physics begins with the hydrogen atom. In this case, the most basic system is the pure AB diblock copolymer melt, where the molecule is composed of just two sequential blocks denoted A and B. For theoretical purposes, it is advantageous to group monomers together into larger units called segments, each with the same specified volume, ρ_0^{-1}. The AB diblock copolymer is then characterized by its total number of such segments, N, and the fraction, f, of those that are of type A.

Block copolymer melts are blessed with a number of distinct advantages over small-molecule lyotropic systems. For example, the macromolecular nature of polymers suppresses effects related to the atomic details, providing systems where the behaviour is more universal and dependent upon far fewer parameters. In particular, high-molecular-weight polymers can be accurately modelled as Gaussian chains, where they are represented by smooth space curves with a simple stretching energy to treat their local configurational entropy, and the molecular interactions between A and B segments can be represented by a single Flory–Huggins χ parameter. Furthermore, the macromolecular character suppresses fluctuation effects, which tend to obscure the underlying mechanisms responsible for molecular self-assembly. The absence of fluctuations also implies that mean-field results are accurate. This has been particularly valuable now that new advances in self-consistent field theory (SCFT) [3,4] permit exact mean-field calculations for arbitrarily complex ordered microstructures [5].

When the incompatibility of unlike segments, as determined by the product, χN, becomes sufficient, the segments segregate into A- and B-rich domains forming periodically ordered microstructures like those depicted in figure 1. Amazingly, these structures are virtually identical to those of the conventional lyotropic systems [1]. The simplest and most common *classical* microstructures, include the lamellar (L) phase in which the domains form alternating flat layers, the cylindrical (C) phase where the minority component forms cylinders packed on a hexagonal lattice, and the spherical (S) phase where the minority blocks form spheres arranged on a bcc lattice. We will also discuss the variation where the spheres occur on a close-packed lattice (S_{cp}). The molecular self-assembly also produces more *complex* microstructures, the most common being the gyroid (G) phase where the minority domain forms two interweaving three-fold coordinated lattices [6, 7]. Experiments have also identified a perforated-lamellar (PL) phase similar to the classical L phase, but with a hexagonal arrangement of perforations in the thinner minority layers through which the majority layers are connected [8]. For neat diblock copolymer melts, this state is only metastable and eventually converts to the G phase after sufficient annealing [9, 10]. Another structure occasionally observed in conventional lyotropics is the double-diamond (D) phase similar to G, but where the interweaving lattices are four-fold coordinated [1]. However, this structure is absent from the neat diblock system [11].

Figure 2 compares the mean-field phase diagram [12] for diblock copolymers to experiment [13–15][1]. Despite the clear similarities, there are some significant differences. The qualitative differences along the order–disorder transition (ODT) are attributed to fluctuation

[1] The experimental PS–PI phase diagram in figure 2(b) has been revised from the original [13–15] by interpreting PL as a metastable state that eventually converts to G after sufficient annealing [9].

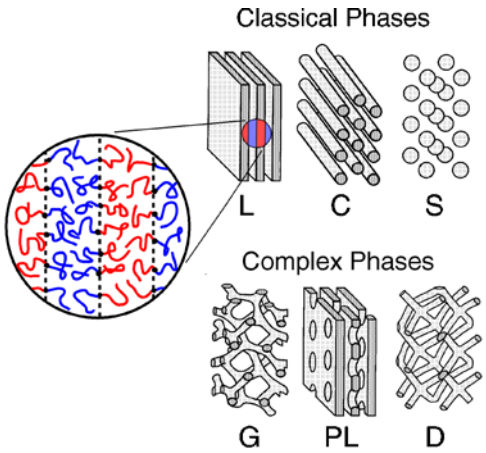

Figure 1. Schematic illustrations of six ordered morphologies showing the domains occupied by the smaller minority blocks. The morphologies can be subdivided into the classical lamellar (L), cylindrical (C) and spherical (S) phases, and the complex gyroid (G), perforated-lamellar (PL) and double-diamond (D) phases. The expanded view of the L phase demonstrates the self-assembly of individual molecules within the morphology.

effects omitted by the mean-field calculation [16]. The experimental diagram also possesses a small degree of asymmetry about $f = 0.5$, which is partly accounted for by the asymmetry in the A and B statistical segment lengths [17]. Naturally, some of the differences can be attributed to the standard Gaussian model, but we should also acknowledge a significant degree of experimental inaccuracy in figure 2(b) due to nonequilibrium effects, uncertainties in molecular characteristics, impurities, etc. Considering all this, the theory is, in fact, rather successful. Most importantly, the theory has contributed greatly to our fundamental understanding of these molecules by providing simply intuitive explanations for the qualitative features of the phase diagram, including the absence of the D and PL phases.

The present literature already contains a number of valuable reviews [12, 13, 18–22] and books [23–25] on block copolymer systems. This review aims to compliment them by providing an introduction to block copolymer theory in the context of the simple diblock copolymer melt. The task of doing so is greatly simplified by the fact that researchers have, in most part, embraced a single *standard* model. The success of this model can be attributed to its microscopic origin combined with the coarse-graining that buries the complications associated with treating atomic details. Section 2 provides a complete description of the model and justifies the underlying assumptions. Despite its simplicity, the fact that the model considers individual molecules renders an exact statistical mechanical treatment untractable. Fortunately, the suppression of fluctuations in polymeric systems permits accurate results to be obtained using the mean-field method. Section 3 describes the exact numerical implementation of mean-field theory as well as analytic approximations for both weakly and strongly segregated melts. We present these in a unified framework opting for slightly more intuitive derivations over the more traditional rigorous ones. From the theory, there emerge simple intuitive explanations for block copolymer phase behaviour, to which we devote section 4. Although reasonably accurate, the mean-field results are modified by fluctuation effects discussed in section 5. The review concludes with section 6 discussing some of the outstanding problems facing the future progress of block copolymer research.

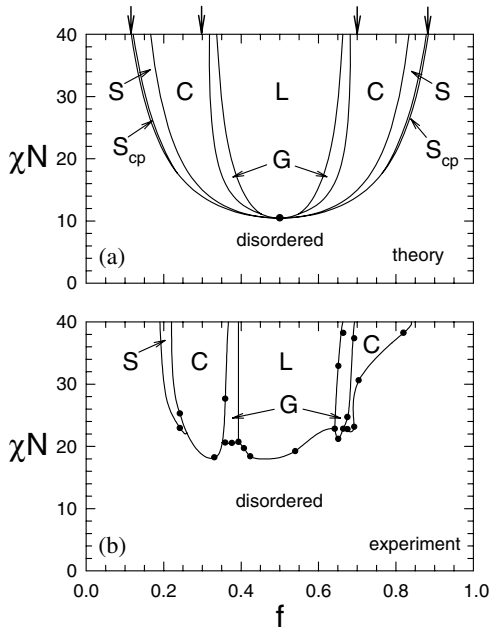

Figure 2. (a) Theoretical and (b) experimental equilibrium phase diagrams calculated using SCFT and measured using polystyrene–polyisoprene diblock copolymers. In (a), the solid dot denotes the mean-field critical point and the vertical arrows indicate the L/C and C/S phase boundaries as predicted by SST. In (b), the solid dots denote the experimental data points, while the curves serve only as a guide to the eye. Plots (a) and (b) are adapted from [12] and [13–15], respectively.

2. Model

It is immensely convenient that block copolymer theory has largely evolved around a common standard model, particularly as this allows easy comparison between distinct calculations. The chosen model considers the individual molecules, but ignores their atomic structure as this is irrelevant to the mesoscale behaviour of the melt. The wide spread use of this coarse-grained microscopic model has resulted due to its combination of simplicity and validity. Here, we describe it for a melt of n identical AB diblock copolymer molecules, each with N segments of which a fraction f forms the A block. To specify their configurations, each molecule is parametrized by a variable s than increases continuously from 0 to 1 along its length. The configuration of the αth molecule is then represented by a simple mathematical space curve, $\boldsymbol{r}_\alpha(s)$. Given this definition, the concentrations of A and B segments at a given point $\boldsymbol{r}$ are

$$\hat{\phi}_A(\boldsymbol{r}) = \frac{N}{\rho_0}\sum_{\alpha=1}^{n}\int_0^f \delta(\boldsymbol{r}-\boldsymbol{r}_\alpha(s))\,\mathrm{d}s \tag{1}$$

$$\hat{\phi}_B(\boldsymbol{r}) = \frac{N}{\rho_0}\sum_{\alpha=1}^{n}\int_f^1 \delta(\boldsymbol{r}-\boldsymbol{r}_\alpha(s))\,\mathrm{d}s \tag{2}$$

respectively. These concentrations are made dimensionless by dividing by the average segment density, ρ_0. Although $\hat{\phi}_A(\boldsymbol{r})$ and $\hat{\phi}_B(\boldsymbol{r})$ are highly discontinuous functions, owing to the fact that the polymers are treated as infinitely thin threads, their ensemble averages,

$$\phi_A(\boldsymbol{r}) \equiv \langle\hat{\phi}_A(\boldsymbol{r})\rangle \tag{3}$$

$$\phi_B(\boldsymbol{r}) \equiv \langle\hat{\phi}_B(\boldsymbol{r})\rangle \tag{4}$$

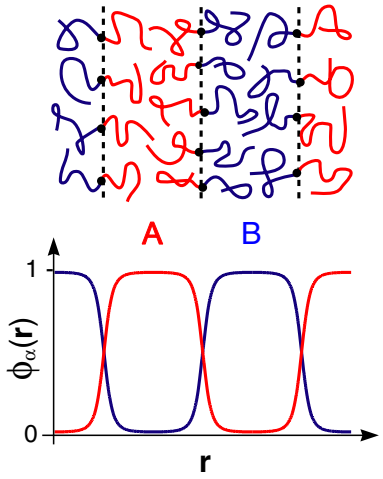

Figure 3. Schematic diagram showing the molecular self-assembly within the lamellar (L) phase with the corresponding ensemble-averaged segment distributions, $\phi_A(\boldsymbol{r})$ and $\phi_B(\boldsymbol{r})$.

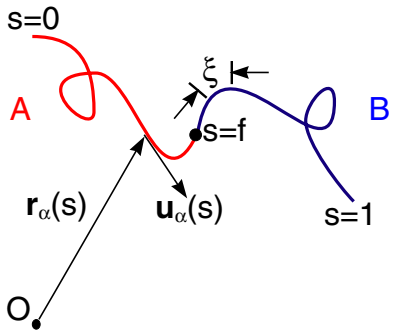

Figure 4. Diagram of a semiflexible worm-like chain with the space curve, $\boldsymbol{r}_\alpha(s)$, specifying its trajectory relative to some arbitrary origin, O, and the unit vector, $\boldsymbol{u}_\alpha(s)$, specifying its local orientation. In this model, the chain has a fixed length, bN, and a bending rigidity, κ, that keeps it relatively straight over a persistence length, $\xi = b\kappa$.

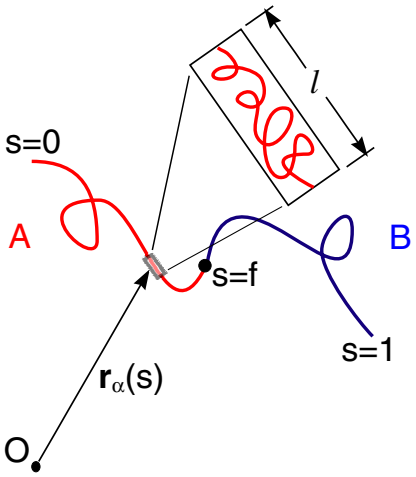

Figure 5. Diagram of a flexible Gaussian chain with the space curve, $\boldsymbol{r}_\alpha(s)$, specifying its trajectory relative to some arbitrary origin, O. In this model, a coarse-grained segment represents a coil of chain, and thus its length, l, can vary. However, the entropy of a segment decreases as it stretches, resulting in a free energy penalty that causes the segment to mimic an ideal spring.

are well-behaved continuous functions. These average concentrations are plotted for the lamellar (L) phase in figure 3.

2.1. Incompressibility

Molecular interactions are typically separated into a short-range hard-core repulsion and a long-range attraction. The primary effect of the hard-core component is to prevent the molecules from overlapping, which is responsible for the near incompressibility of a liquid. Indeed, high-pressure experiments [26] on block copolymer melts have demonstrated a negligible compressibility. This fact permits us to simplify the model by imposing an incompressibility

assumption,

$$\hat{\phi}_A(\boldsymbol{r}) + \hat{\phi}_B(\boldsymbol{r}) = 1 \tag{5}$$

in place of the hard-core interactions. Of course, we cannot strictly enforce such an incompressibility if we treat the molecules as infinitely thin threads, but it can be enforced on all length scales down to some microscopic cutoff. Nevertheless, this issue becomes irrelevant in mean-field theory, because the theory is only capable of constraining the ensemble-averaged concentrations, i.e.

$$\phi_A(\boldsymbol{r}) + \phi_B(\boldsymbol{r}) = 1. \tag{6}$$

2.2. Segment interactions

Given the incompressibility assumption, the model only needs to consider the attractive portion of the interaction. Although this part of the interaction is long-range relative to the hard-core part, it is nevertheless short-range compared to the dimensions of any microstructure within the melt. Therefore, the attractions can be treated by simple contact forces. In a small volume, $\mathrm{d}\boldsymbol{r}$, located at $\boldsymbol{r}$, the number of A/B segment contacts is assumed to be proportional to the product, $\hat{\phi}_A(\boldsymbol{r})\hat{\phi}_B(\boldsymbol{r})\,\mathrm{d}\boldsymbol{r}$. Hence, the total internal energy of the melt is

$$\frac{\hat{U}}{k_\mathrm{B}T} = \chi\rho_0 \int \hat{\phi}_A(\boldsymbol{r})\hat{\phi}_B(\boldsymbol{r})\,\mathrm{d}\boldsymbol{r} \tag{7}$$

where χ is a proportionality constant that varies with temperature. The thermal energy $k_\mathrm{B}T$ and segment density ρ_0 are included to make χ dimensionless. Note that there is no need to include analogous integrals for the A/A and B/B segment interactions provided the melt is treated as incompressible, because the incompressibility condition can be used to reexpress each of them as an irrelevant constant plus an integral equivalent to the above.

2.3. Semiflexible worm-like chain

The last consideration is the internal energy of the polymer chain. Rather than first discussing the simple Gaussian model upon which most calculations are based, we begin with a slightly more complicated but more realistic and intuitive model known as the worm-like chain [27–30]. In this model, each segment has a fixed contour length, b, and a finite bending rigidity, κ. The bending energy of the polymer backbone over an interval, $s_1 < s < s_2$, is given by the integral,

$$\frac{\hat{E}_b[\boldsymbol{r}_\alpha(s); s_1, s_2]}{k_\mathrm{B}T} = \frac{\kappa}{2N}\int_{s_1}^{s_2} |\boldsymbol{u}'_\alpha(s)|^2\,\mathrm{d}s \tag{8}$$

where $\boldsymbol{u}_\alpha(s) \equiv \boldsymbol{r}'_\alpha(s)/bN$ is the unit vector tangent to the chain as indicated in figure 4. Clearly, a large bending rigidity κ suppresses variations in $\boldsymbol{u}_\alpha(s)$ or, in other words, opposes bending. The persistence length over which the chain remains relatively straight is given by $\xi = b\kappa$. Thus, by tuning κ, this model can span continuously between the rigid-rod limit ($\xi \gg bN$) and the flexible-chain limit ($\xi \ll bN$) characteristic of high-molecular-weight polymers. Note that, if one wishes to assign distinct contour lengths, b_A and b_B, or distinct bending rigidities, κ_A and κ_B, to the A and B segments, respectively, it is just a simple matter of splitting the integral (8) for $s < f$ and $s > f$.

2.4. Flexible Gaussian chain

Although manageable, the worm-like chain model is unnecessarily complicated when considering high-molecular-weight polymers where $\xi \ll bN$. If we let $\xi \to 0$ and $b \to \infty$

while at the same time $(2\xi b)^{1/2}$ approaches a finite value, a, we end up with the Gaussian chain model. The value a is referred to as the statistical segment length, and is effectively the RMS end-to-end length of a unperturbed segment. Provided that the segment profiles, $\phi_A(\boldsymbol{r})$ and $\phi_B(\boldsymbol{r})$, vary slowly relative to the persistence length, ξ, the Gaussian model is equivalent to the worm-like model but much simpler to apply.

One small difficulty with letting the persistence length approach zero is that the polymer trajectory becomes extremely erratic making it impossible to specify the chain orientation. To cope with this, the space curves, $\boldsymbol{r}_\alpha(s)$, are redefined as smooth coarse-grained paths through the N segments of the chain as in figure 5. On this scale, the segments appear relatively straight as in the worm-like chain model, but now their length, l, can vary due to their internal coil-like structure. However, as an individual coarse-grained segment stretches, the number of available internal configurations decreases. The corresponding drop in entropy produces a free energy penalty that opposes the stretching. In fact, the entropic free energy increases as l^2, and hence a Gaussian segment behaves equivalently to an ideal spring [31]. The total stretching energy for a given interval, $s_1 < s < s_2$, of the chain is

$$\frac{\hat{E}_{st}[\boldsymbol{r}_\alpha(s); s_1, s_2]}{k_\mathrm{B}T} = \frac{3}{2Na^2}\int_{s_1}^{s_2} |\boldsymbol{r}'_\alpha(s)|^2 \,\mathrm{d}s \tag{9}$$

where a^{-2} acts as a spring constant. Again, the A and B segments can be assigned distinct statistical lengths, a_A and a_B, respectively, by simply splitting the integral (9) into two parts [17].

2.5. Extensions to the model

The standard Gaussian model described above has dominated because of its inherent simplicity. Nevertheless, many generalizations are straightforward. For example, the internal energy can be expanded as

$$\frac{\hat{U}}{k_\mathrm{B}T} = \rho_0 \int [-\chi\hat{\phi}^2(\boldsymbol{r}) + \chi_3\hat{\phi}^3(\boldsymbol{r}) + \chi_4\hat{\phi}^4(\boldsymbol{r}) + \cdots]\,\mathrm{d}\boldsymbol{r} \tag{10}$$

where $\hat{\phi}(\boldsymbol{r}) \equiv \hat{\phi}_A(\boldsymbol{r}) - f$. The linear term is omitted because it integrates to zero, and the second-order term is written such that the expression becomes equivalent to equation (7) when $\chi_3 = \chi_4 = \cdots = 0$. The addition of higher-order terms is analogous to providing the normal Flory–Huggins χ parameter with a concentration dependence [32]. Still, this expression (10) is limited to local interactions of zero range. Short-range interactions can be incorporated by supplementing the internal energy with the non-local term,

$$\frac{\hat{U}_{nl}}{k_\mathrm{B}T} = -\frac{1}{6}\chi\sigma^2\rho_0 \int |\nabla\hat{\phi}(\boldsymbol{r})|^2 \,\mathrm{d}\boldsymbol{r} \tag{11}$$

where σ measures the range of the interaction [3]. Realistic interactions also possess some orientational dependence. Unfortunately, a proper treatment of such nematic interactions is impossible in the Gaussian chain model, because the chain orientation is completely lost. Nevertheless, it is easily incorporated into the worm-like chain model [27]. It is clear that such interactions are essential for copolymers containing liquid-crystalline units, but they may also have a significant effect in conventional block copolymer melts. The incompressibility constraint is easily relaxed [4], but this introduces additional parameters, specifically the compressibilities of the A and B segments. The versatility of the model also extends to more complex architectures, such as ABA triblocks [33], linear multiblocks [34], starblocks [35], ABC triblocks [36], etc. Furthermore, there is absolutely no difficulty in considering a blend involving various block copolymers, homopolymers, and solvents [37, 38].

3. Mean-field theory

According to the standard Gaussian model, diblock copolymers are treated as microscopic elastic threads with two ends that interact by an unfavourable contact energy under the constraint that they must fill space uniformly. Despite the simplicity of this model, the statistical mechanics required to predict the equilibrium behaviour is still complicated by the correlations associated with interacting molecules. To cope with this many-body problem, it is useful to replace the interactions by the fields,

$$\hat{w}_A(\boldsymbol{r}) = \chi N \hat{\phi}_B(\boldsymbol{r}) + \hat{\xi}(\boldsymbol{r}) \tag{12}$$

$$\hat{w}_B(\boldsymbol{r}) = \chi N \hat{\phi}_A(\boldsymbol{r}) + \hat{\xi}(\boldsymbol{r}) \tag{13}$$

representing the total interaction experienced by individual A and B *test* segments, respectively, at position $\boldsymbol{r}$. In each case, the first term represents the attractive portion of the molecular interactions, while the second represents the hard-core part. Of course, we have replaced the latter interactions by the incompressibility constraint, and so $\hat{\xi}(\boldsymbol{r})$ is actually the Lagrange-multiplier field enforcing the constraint, but nevertheless it can be interpreted as the field due to hard-core interactions.

Thus far, no approximations have been made. However, we are prevented from proceeding by the fact the fields fluctuate due to the motion of the molecules creating them. In mean-field theory, this is remedied by simply time averaging (or equivalently ensemble averaging) the field equations

$$w_A(\boldsymbol{r}) = \chi N \phi_B(\boldsymbol{r}) + \xi(\boldsymbol{r}) \tag{14}$$

$$w_B(\boldsymbol{r}) = \chi N \phi_A(\boldsymbol{r}) + \xi(\boldsymbol{r}) \tag{15}$$

where $\xi(\boldsymbol{r})$ is to be determined by equation (6). The mean fields are plotted in figure 6 for a simple lamellar (L) phase.

By appreciating that the mean-field method simply involves approximating the instantaneous fields, $\hat{w}_A(\boldsymbol{r})$ and $\hat{w}_B(\boldsymbol{r})$, by their time averages, $w_A(\boldsymbol{r})$ and $w_B(\boldsymbol{r})$, it is easy to understand its implications and limitations. For instance, mean-field theory is accurate for well-ordered microstructures since the fields are large relative to their thermal fluctuations. It is also accurate deep in the disordered region, but in this case because the fields are so weak that any approximation would do. The inaccuracies in mean-field theory are most significant near the ODT, where the fields are highly fluctuating and sufficiently strong to affect the polymer configurations.

3.1. Self-consistent field theory

The full mean-field theory, more commonly referred to as SCFT, was first extended to block copolymers by Helfand [3,4] in 1975. Here, we present an alternative derivation that is a little less rigorous but more intuitive. The essential part of SCFT is evaluating the exact equilibrium behaviour of a single diblock copolymer subjected to the mean fields, $w_A(\boldsymbol{r})$ and $w_B(\boldsymbol{r})$. The partition function for this is

$$\mathcal{Q} = \sum_{\boldsymbol{r}_\alpha(s)}^{0<s<1} \exp\left\{-\frac{\hat{E}_{mf}[\boldsymbol{r}_\alpha(s);0,1]}{k_{\mathrm{B}}T}\right\} \tag{16}$$

where the sum is over all space curves $\boldsymbol{r}_\alpha(s)$ with s in the interval $(0,1)$. The energy of a molecule subjected to the mean fields is given by

$$\frac{\hat{E}_{mf}[\boldsymbol{r}_\alpha(s);s_1,s_2]}{k_{\mathrm{B}}T} = \int_{s_1}^{s_2}\left[\frac{3}{2Na^2}|\boldsymbol{r}'_\alpha(s)|^2 + w(\boldsymbol{r}_\alpha(s),s)\right]\mathrm{d}s \tag{17}$$

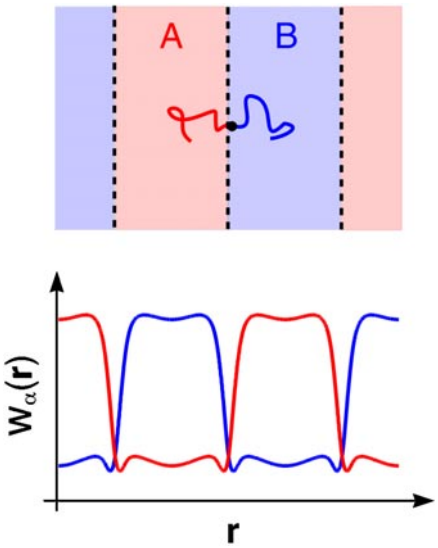

Figure 6. To cope with a large number of interacting molecules, mean-field theory focuses on a single molecule and represents its interactions by two static fields, $w_A(\boldsymbol{r})$ and $w_B(\boldsymbol{r})$, acting on the A and B segments, respectively.

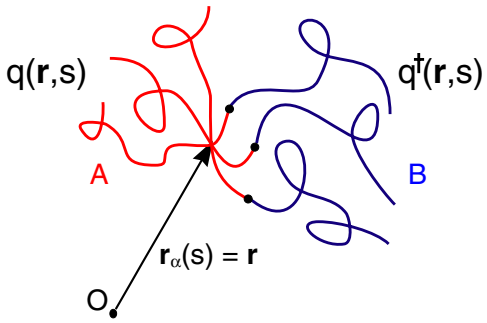

Figure 7. Three representative configurations of a diblock molecule with its s segment fixed at position $\boldsymbol{r}$. Given that the molecule is exposed to static fields, the energies of the two portions, $(0, s)$ and $(s, 1)$, are uncoupled, permitting us to calculate their individual partition functions, $q(\boldsymbol{r}, s)$ and $q^\dagger(\boldsymbol{r}, s)$, respectively. The total partition function for the constrained chain is then the product, $q(\boldsymbol{r}, s)q^\dagger(\boldsymbol{r}, s)$.

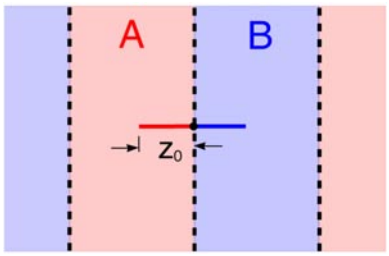

Figure 8. At extreme segregations, the coarse-grained trajectory of a diblock molecule is restricted to straight paths normal to the interface. Nevertheless, the molecules still exhibit a nontrivial distribution of block lengths, z_0.

where for convenience we have defined

$$w(\boldsymbol{r}, s) \equiv \begin{cases} w_A(\boldsymbol{r}) & \text{if} \quad s < f \\ w_B(\boldsymbol{r}) & \text{if} \quad f < s. \end{cases} \tag{18}$$

In order to evaluate $\mathcal{Q}$, we first calculate the partition function

$$\mathcal{Q}_c(\boldsymbol{r}, s) = \sum_{\boldsymbol{r}_\alpha(t)}^{0<t<1} \exp\left\{-\frac{\hat{E}_{mf}[\boldsymbol{r}_\alpha(t); 0, 1]}{k_B T}\right\} \delta(\boldsymbol{r}_\alpha(s) - \boldsymbol{r}) \tag{19}$$

for a diblock copolymer with the sth segment constrained to position $\boldsymbol{r}$. Since the energy of the chain can be split as

$$\hat{E}_{mf}[\boldsymbol{r}_\alpha(t); 0, 1] = \hat{E}_{mf}[\boldsymbol{r}_\alpha(t); 0, s] + \hat{E}_{mf}[\boldsymbol{r}_\alpha(t); s, 1] \tag{20}$$

$\mathcal{Q}_c(\boldsymbol{r}, s)$ can be expressed as the product of two partial partition functions,

$$q(\boldsymbol{r}, s) = \sum_{\boldsymbol{r}_\alpha(t)}^{0<t<s} \exp\left\{-\frac{\hat{E}_{mf}[\boldsymbol{r}_\alpha(t); 0, s]}{k_\mathrm{B}T}\right\} \delta(\boldsymbol{r}_\alpha(s) - \boldsymbol{r}) \tag{21}$$

$$q^\dagger(\boldsymbol{r}, s) = \sum_{\boldsymbol{r}_\alpha(t)}^{s<t<1} \exp\left\{-\frac{\hat{E}_{mf}[\boldsymbol{r}_\alpha(t); s, 1]}{k_\mathrm{B}T}\right\} \delta(\boldsymbol{r}_\alpha(s) - \boldsymbol{r}) \tag{22}$$

as illustrated by figure 7. The first, $q(\boldsymbol{r}, s)$, can be evaluated starting from $q(\boldsymbol{r}, 0) = 1$ and iterating with

$$q(\boldsymbol{r}, s + \varepsilon) = \int q(\boldsymbol{r} + \boldsymbol{R}, s) \exp\left\{-\frac{3|\boldsymbol{R}|^2}{2Na^2\varepsilon} - \epsilon w(\boldsymbol{r}, s)\right\} \mathrm{d}\boldsymbol{R} \tag{23}$$

using a sufficiently small ε. Alternatively, equation (23) can be converted to the differential equation [3],

$$\frac{\partial}{\partial s} q(\boldsymbol{r}, s) = \frac{a^2 N}{6} \nabla^2 q(\boldsymbol{r}, s) - w(\boldsymbol{r}, s) q(\boldsymbol{r}, s). \tag{24}$$

The equation for $q^\dagger(\boldsymbol{r}, s)$ is identical, but with the right-hand side multiplied by -1. Given the partition function, $\mathcal{Q}_c(\boldsymbol{r}, s) = q(s, \boldsymbol{r}) q^\dagger(s, \boldsymbol{r})$, for a constrained chain, the partition function, $\mathcal{Q}$, for an unconstrained chain is evaluated by summing over all possible positions $\boldsymbol{r}$ of the sth segment;

$$\mathcal{Q} = \int q(s, \boldsymbol{r}) q^\dagger(s, \boldsymbol{r}) \, \mathrm{d}\boldsymbol{r}. \tag{25}$$

As must be the case, the above integral is independent of s. The constrained partition function $\mathcal{Q}_c(\boldsymbol{r}, s)$ also serves a second purpose as it is directly proportional to the distribution of the sth segment. From this and the fact that the volume average of $\phi_A(\boldsymbol{r})$ must equal f, it immediately follows that

$$\phi_A(\boldsymbol{r}) = \frac{V}{\mathcal{Q}} \int_0^f q(s, \boldsymbol{r}) q^\dagger(s, \boldsymbol{r}) \, \mathrm{d}s. \tag{26}$$

The expression for $\phi_B(\boldsymbol{r})$ is identical, except that the integral extends from f to 1. Because ordered block copolymer morphologies are periodic, it is most efficient to perform the above calculation using the Fourier-space algorithm developed in [5].

Now that we can evaluate $\phi_A(\boldsymbol{r})$ and $\phi_B(\boldsymbol{r})$ for any given $w_A(\boldsymbol{r})$ and $w_B(\boldsymbol{r})$, the next step is to adjust the fields according to an iterative procedure[2] so as to satisfy the self-consistent equations (14), (15) and the incompressibility condition (6). However, there are an infinity of possible solutions, each corresponding to a different morphology. Based on experiment and our intuition, we often know which morphologies to consider, and then it is just a matter of locating their appropriate solutions. A desired solution is obtained by starting the iteration from a sensible initial guess, where the minima of $w_A(\boldsymbol{r})$ and $w_B(\boldsymbol{r})$ correspond to the expected locations of the A and B domains, respectively. In the event that not all the possible morphologies are known, a real-space screening method introduced by Drolet and Fredrickson [42] can be used to generating new candidate structures.

To identify which solution represents the equilibrium morphology as well as to determine its preferred domain spacing requires the free energy, $F = U - TS$. In the spirit of mean-field theory, the average internal energy is approximated by

$$\frac{U}{k_\mathrm{B}T} = \chi\rho_0 \int \phi_A(\boldsymbol{r}) \phi_B(\boldsymbol{r}) \, \mathrm{d}\boldsymbol{r}. \tag{27}$$

[2] Usually the iteration is performed by a quasi-Newton–Raphson method or by a Picard procedure as described in [39].

The entropy is then obtained by taking the free energy of n diblock copolymers subjected to the mean fields, and subtracting off the energy of the fields;

$$\frac{S}{k_B} = n \ln \mathcal{Q} + \rho_0 \int [w_A(\boldsymbol{r})\phi_A(\boldsymbol{r}) + w_B(\boldsymbol{r})\phi_B(\boldsymbol{r})]\, \mathrm{d}\boldsymbol{r}. \tag{28}$$

The theoretical phase diagram in figure 2(a) is nothing more than a map showing the morphology of lowest free energy plotted as a function of segregation χN and composition f.

3.2. Weak-segregation theory

In 1980, Leibler [43] introduced an analytical approximation to the full mean-field theory appropriate for weakly-segregated melts. This was done by deriving a Landau expansion about the disordered state,

$$\begin{aligned}\frac{F[\phi]}{nk_BT} \approx \chi N f(1-f) &+ \frac{V}{2!(2\pi)} \int S^{-1}(\boldsymbol{q}_1)\phi(\boldsymbol{q}_1)\phi(-\boldsymbol{q}_1)\, \mathrm{d}\boldsymbol{q}_1 \\ &+ \frac{V^2}{3!(2\pi)^2} \int \Gamma_3(\boldsymbol{q}_1, \boldsymbol{q}_2)\phi(\boldsymbol{q}_1)\phi(\boldsymbol{q}_2)\phi(-\boldsymbol{q}_1 - \boldsymbol{q}_2)\, \mathrm{d}\boldsymbol{q}_1\, \mathrm{d}\boldsymbol{q}_2 \\ &+ \frac{V^3}{4!(2\pi)^3} \int \Gamma_4(\boldsymbol{q}_1, \boldsymbol{q}_2, \boldsymbol{q}_3)\phi(\boldsymbol{q}_1)\phi(\boldsymbol{q}_2)\phi(\boldsymbol{q}_3)\phi(-\boldsymbol{q}_1 - \boldsymbol{q}_2 - \boldsymbol{q}_3)\, \mathrm{d}\boldsymbol{q}_1\, \mathrm{d}\boldsymbol{q}_2\, \mathrm{d}\boldsymbol{q}_3\end{aligned} \tag{29}$$

to fourth-order in the Fourier transform of the concentration profile,

$$\phi(\boldsymbol{q}) = \frac{1}{V} \int [\phi_A(\boldsymbol{r}) - f] \exp(\mathrm{i}\boldsymbol{r} \cdot \boldsymbol{q})\, \mathrm{d}\boldsymbol{r}. \tag{30}$$

The mean-field free energy, F, of the melt is found by minimizing this functional, $F[\phi]$, with respect to the concentration profile, $\phi(\boldsymbol{q})$.

In the limit of weakly-segregated melts, the phase behaviour is governed by the inverse scattering function,

$$S^{-1}(\boldsymbol{q}) = F(q^2a^2N/6) - 2\chi N \tag{31}$$

where

$$F(x) = g(1, x)/[g(f, x)g(1-f, x) - h^2(f, x)h^2(1-f, x)] \tag{32}$$

$$g(s, x) = 2[sx + \exp(-sx) - 1]/x^2 \tag{33}$$

$$h(s, x) = [1 - \exp(-sx)]/x. \tag{34}$$

At low χN, $S^{-1}(\boldsymbol{q})$ is positive for all $\boldsymbol{q}$, and therefore the disordered state (i.e. $\phi(\boldsymbol{q}) = 0$) provides the lowest free energy. However, as χN increases, a spinodal curve is encountered at which point $S^{-1}(\boldsymbol{q})$ becomes zero on a spherical shell of radius q^*. Beyond the spinodal curve, the quadratic term favours periodic profiles of wavelength $2\pi/q^*$, causing the disordered phase to become unstable. The quartic term serves to prevent the concentration modulations from diverging. The cubic term has the notable effect of causing the ordered phase (i.e. $\phi(\boldsymbol{q}) \neq 0$) to become stable just prior to the spinodal resulting in a discontinuous ODT. The only exception is for $f = 0.5$, where by symmetry the cubic term is absent, and consequently the ODT becomes a critical point coinciding with the spinodal curve.

In the vicinity of the spinodal, the free energy is dominated by wavevectors, $\boldsymbol{q}$, satisfying $|\boldsymbol{q}| = q^*$. As a result, the only ordered structures are those with either lamellar, hexagonal (p6mm), or body-centred cubic ($Im\bar{3}m$) symmetry [44]. However, beyond the spinodal, additional wavevectors become relevant allowing the formation of, for example, close-packed

spheres (S_{cp}) and gyroid (G) [45]. Note that at the segregations where S_{cp} occurs in figure 2(a), the ODT is well separated from the spinodal curve.

The weak-segregation theory provides a nice explanation for the structure of the mean-field phase diagram in the region surrounding the critical point in figure 2(a), but it becomes seriously inaccurate above $\chi N \approx 12$ [12]. Unfortunately, this small region of the phase diagram is completely modified by fluctuation effects. Although the Leibler functional (29) has served a useful purpose for incorporating fluctuation corrections [16], emerging evidence suggests that it is also inappropriate in this capacity [32]. The expansion (29) does provide the disordered-state scattering function (31), but then SCFT supplies this as well as all the ordered-state scattering functions [46,47]. It may be that the usefulness of this weak-segregation theory has now been exhausted.

3.3. Strong-segregation theory

In 1985, Semenov [48] introduced a theory for generating analytical expressions for the strong-segregation regime, which has proven extremely valuable. In this limit, the A and B segments are completely separated except for a narrow region about the interface, and the chains are so strongly stretched that they follow straight paths perpendicular to the interface as illustrated in figure 8. Of course, they are only straight in the *course-grained* sense; the end-to-end length of a molecule is still assumed to be much smaller than its contour length.

At this level of segregation, the interaction and stretching energies can be treated separately. The free energy of the interface is given by

$$\frac{F_{\rm int}}{k_{\rm B}T} = \rho_0 \mathcal{A} \int_{-\infty}^{\infty} \left[\chi \phi_A(z)\phi_B(z) + \frac{[a\phi'_A(z)]^2}{24\phi_A(z)} + \frac{[a\phi'_B(z)]^2}{24\phi_B(z)} \right] {\rm d}z \tag{35}$$

where $\mathcal{A}$ is the interfacial area and z is a coordinate perpendicular to the interface. The integrand rapidly approaches zero away from the interface at $z = 0$, which allows the limits to be extended to infinity. The first term of the integrand is the interaction energy (27). The second and third terms represent the local configurational entropy loss of the A and B segments, respectively, due to the deviation from random-walk statistics caused by the interface [49]. Minimizing $F_{\rm int}$ under the incompressibility constraint provides the segment profile,

$$\phi_A(z) = \frac{1}{2}\left[1 + \tanh\left(\frac{2z}{w}\right)\right] \tag{36}$$

where $w \equiv 2a/(6\chi)^{1/2}$ is a measure of the interfacial width [48]. Substituting this into equation (35) gives

$$\frac{F_{\rm int}}{k_{\rm B}T} = \rho_0 \mathcal{A} a \left(\frac{\chi}{6}\right)^{1/2}. \tag{37}$$

Now we consider the stretching energy $F^A_{st,\alpha}$ of a single A block. Rather than following the original derivation by Semenov [48], we opt for a simpler one by Milner *et al* [50]. Since the individual block follows a straight path, its space curve, $\boldsymbol{r}_\alpha(s)$, can be replaced by a scalar function, $z_\alpha(s)$, representing the shortest distance from the s segment to the nearest interface. Thus, equation (17) can be rewritten as

$$\frac{\hat{E}_{mf}[z_\alpha(s);\,0,\,f]}{k_{\rm B}T} = \int_0^f \left[\frac{3}{2Na^2}[z'_\alpha(s)]^2 + w_A(z_\alpha(s))\right] {\rm d}s. \tag{38}$$

At high segregation, the partition function is dominated by the lowest-energy configuration, and so we only require the path $z_\alpha(s)$ that minimizes $\hat{E}_{mf}[z_\alpha(s);\,0,\,f]$. Fortunately, this can be found immediately by making an analogy with classical mechanics. If we interpret s as

time and $z_\alpha(s)$ as the position of a particle with mass $3/Na^2$, then equation (38) is the action of the particle in a potential $-w_A(z)$ [51]. The fact our chain cannot sustain a tension at its free end (i.e. $z'_\alpha(0) = 0$), implies the particle starts from rest. Furthermore, the particle must finish at the interface (i.e. $z_\alpha(f) = 0$), regardless of its starting point (i.e. $z_\alpha(0) = z_0$). The only potential that permits all this is the harmonic one,

$$-w_A(z) = \frac{3\pi^2}{8f^2Na^2}z^2. \tag{39}$$

When we substitute the corresponding trajectory,

$$z_\alpha(s) = z_0 \cos(\pi s/2f) \tag{40}$$

into equation (38), we find that the stretching energy exactly cancels the energy of the field to give zero. This allows us to equate the stretching energy to minus the field energy;

$$\begin{aligned}\frac{F^A_{st,\alpha}}{k_\mathrm{B}T} &= \frac{3\pi^2}{8f^2Na^2}\int_0^f [z_\alpha(s)]^2\,\mathrm{d}s,\\ &= \frac{3\pi^2}{8f^2Na^2}\int_0^{z_0} z^2\phi_\alpha(z)\,\mathrm{d}z\end{aligned} \tag{41}$$

where $\phi_\alpha(z) \equiv \mathrm{d}s/\mathrm{d}z$ is the segment concentration at z. If we sum over all A blocks, this concentration must integrate to one by the incompressibility constraint (6), and hence the total stretching energy of all the A blocks is

$$\frac{F^A_{st}}{nk_\mathrm{B}T} = \frac{3\pi^2}{8f^2Na^2V}\int_{V_A} z^2\,\mathrm{d}\boldsymbol{r} \tag{42}$$

where the integral is over the volume, V_A, of the A domain with z representing the shortest distance to an interface. The expression for the B blocks is equivalent, except with f replaced by $1 - f$.

The vertical arrows in figure 2(a) denote the phase boundaries separating the classical phases obtained by comparing their total free energies, $F = F_\mathrm{int} + F^A_{st} + F^B_{st}$, using this strong-segregation theory (SST). SST calculations indicate that the complex phases, G [53,54], PL [55], and D [54, 56, 57], are all unstable consistent with strong-segregation results from SCFT [12, 58] as well as experiment [59]. Still, we must note that, with the exception of the L phase, all SST calculations are supplemented with various approximations. First, they generally do not minimize the free energy with respect to the shape of the interface. Second, the above algorithm neglects the fact the distribution of A and B ends at the interface must exactly match due to the connectivity of the blocks, which can result in unphysical predictions [52]. Third, the algorithm overlooks the occurrence of zones where the chain ends are excluded. Fourth, the shape of Wigner–Seitz unit cell is usually approximated [60]. Likhtman and Semenov [53] have now introduced a more complete derivation that accounts for the first two issues, while Ball *et al* [61] have worked out the effect of exclusion zones for cylindrical interfaces. Nevertheless, even after considering all these known issues, direct comparisons with SCFT at $\chi N \sim 1000$ suggest that our present understanding of the strong-segregation limit is still incomplete [62]. At the very least, it is clear that SST is highly inaccurate at experimentally relevant degrees of segregation. It may be that this can be remedied with finite-segregation corrections. So far, researchers have considered corrections for the junction entropy [63, 64], the entropy of the chain ends [65], chain fluctuations [66], and overcrowding at the interface [67]. Certainly, the valuable insights gained thus far from SST warrant further efforts in this direction.

4. Physics of block copolymer melts

One of the most valuable achievements of block copolymer theory has been the establishment of simple intuitive explanations for the ordered phase behaviour. Below, three physical principals governing this behaviour are discussed in order of importance. Although our discussion is only in the context of bulk diblock copolymer melts, these powerful concepts apply to virtually all block copolymer systems. To conclude this section, these principals are used to explain the effect of conformational asymmetry where $a_A \neq a_B$.

4.1. Interfacial area per molecule

The primary concern in a block copolymer melt is the interfacial area per molecule, $\Sigma \equiv \mathcal{A}/n$. This issue is best addressed by considering the simple lamellar phase in the framework of SST, where the A and B chains form two brushes of heights, $h_{A,0}$ and $h_{B,0}$, respectively. Assuming incompressibility,

$$h_{A,0} = fN/\Sigma\rho_0, \tag{43}$$

$$h_{B,0} = (1-f)N/\Sigma\rho_0. \tag{44}$$

Given that, the free energy F of the lamellar phase is

$$\frac{F}{nk_{\mathrm{B}}T} = \Sigma\rho_0 a\left(\frac{\chi}{6}\right)^{1/2} + \frac{\pi^2 N}{8\Sigma^2\rho_0^2 a^2}. \tag{45}$$

The first term, representing the interfacial energy, follows immediately from equation (37), while the second term, representing the total stretching energy, is obtained from equation (42) combined with the analogous expression for the B domain. Clearly, the interfacial energy term favours small Σ, whereas the stretching energy term prefers large Σ. This competition leads to the equilibrium area,

$$\Sigma = \frac{N^{1/2}}{\rho_0 a}\left(\frac{3\pi^4}{8\chi N}\right)^{1/6} \tag{46}$$

determined by minimizing the free energy (45). Careful examination reveals that, in equilibrium, the interfacial energy is twice the stretching energy, which emphasizes that both energy contributions will always be of comparable importance in a well-segregated morphology.

4.2. Spontaneous curvature

If the diblock copolymers are symmetric (i.e. $f = 0.5$), then the A- and B-block stretching energies are balanced and the molecules prefer to pack along flat interfaces. However, if the molecule is asymmetric, then it becomes favourable to curve the interface towards the minority domain. Although this requires the short minority blocks to stretch, the cost is more than compensated for by the relaxation of the larger blocks. This development of spontaneous curvature is nicely demonstrated with a simple SST calculation.

For simplicity, we assume a fixed interfacial area per molecule, Σ, and specify the interfacial curvature, H, as defined in figure 9. Nevertheless, the area available to each molecule does generally change as its trajectory moves away from the interface, as demonstrated by figure 10. Specifically, the area varies as $\Sigma(1-2Hz)$, where z is a coordinate normal to the interface defined to be positive in the A domain and negative in the B domain. Given this, the incompressibility of the A blocks requires

$$\int_0^{h_A} (1-2Hz)\,\mathrm{d}z = fN/\Sigma\rho_0 \tag{47}$$

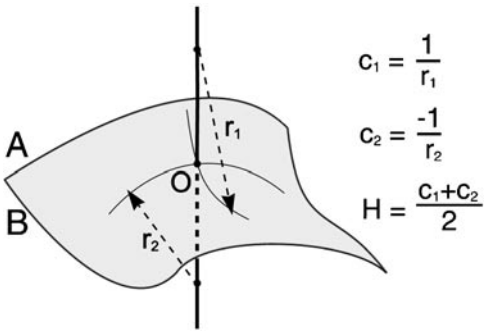

Figure 9. Diagram illustrating how the mean curvature, H, of the A/B interface is calculated at an arbitrary point, O. The shape of the interface is fit to a circular arc passing through O with its centre of curvature lying on the normal. The curvature of the arc is defined as $c = \pm 1/r$, where r is the radius of the arc. We assume a sign convention, where $c > 0$ if the centre of the arc lies on the A side of the interface, and $c < 0$ otherwise. As the arc is rotated about O, the curvature varies between two extreme values, c_1 and c_2, referred to as the principal curvatures, from which H is derived. In this particular example, $c_1 > 0$ and $c_2 < 0$.

which leads to a brush height,

$$h_A \approx h_{A,0}(1 + Hh_{A,0}) \tag{48}$$

where the height for a flat interface, $h_{A,0}$, is given by equation (43). The A-block stretching energy now becomes

$$\begin{aligned} \frac{F_{st}^A}{nk_BT} &= \frac{3\pi^2\Sigma\rho_0}{8f^2N^2a^2}\int_0^{h_A}(1-2Hz)z^2\,\mathrm{d}z \\ &\approx \frac{fF_{st,0}}{nk_BT}\left(1+\frac{3}{2}Hh_{A,0}\right) \\ &= \frac{fF_{st,0}}{nk_BT}\left(1+\frac{3}{2}HfN/\Sigma\rho_0\right) \end{aligned} \tag{49}$$

where $F_{st,0}$ is the total stretching energy for a flat interface, i.e. the second term in equation (45). Combining this with the analogous expression for the B block gives the total stretching energy,

$$F_{st} = F_{st,0}(1 - \tfrac{3}{2}(1-2f)HN/\Sigma\rho_0) \tag{50}$$

to first order in curvature. Provide $f \neq 0.5$, the free energy is a monotonically decreasing function of H, which favours $H \to \infty$ when $f < 0.5$, and $H \to -\infty$ when $f > 0.5$. The higher-order terms that have been neglected provide a restoring force preventing the curvature from actually diverging, thus resulting in a finite preferred curvature.

This preferred or rather spontaneous curvature, H_0, varies monotonically from positive to negative as f increases, passing through zero at $f = 0.5$. The melt tries to match its average interfacial curvature, $\langle H \rangle$, to the spontaneous curvature, H_0, the best it can under the constraint that it must select a space-filling structure. Figure 11 plots the resulting variation in $\langle H \rangle$ as a function of f at $\chi N = 20$. Naturally, the L phase is selected at $f = 0.5$, because it has zero interfacial curvature. In fact, L remains stable down to $f = 0.3745$, simply because no other structure offers an adequately small $\langle H \rangle$. When H_0 becomes sufficiently large, the melt switches to the G phase and then to the more highly curved C and S phases.

4.3. Packing frustration

Based on the spontaneous-curvature argument alone, we might expect the phase sequence L → PL → G → D → C → S. However, the PL and D phases are clearly omitted from the equilibrium phase diagram [9, 11]. In reality, we have overlooked an infinity of other possible structures all of which are ignored by diblock copolymer melts. There is obviously something more to the physics of their behaviour.

We know that the interfacial energy acts to minimize its area under the constraint that the volume fraction of both domains is fixed by the composition, f. Thomas and co-workers [68] have pointed out that this favours uniform interfacial curvature. It is this same tendency that causes soap bubbles to form spheres. However, in block copolymer melts, the stretching energy must also be considered. As our intuition tell us, when stretching ordinary identical springs connected in series, all the springs maintain equal lengths. Since the blocks behave as identical springs, they will also prefer to distribute their stretching energy evenly by forming brushes of uniform thickness. In general, microstructures are unable to accommodate both of these tendencies simultaneously. This inability is referred to as packing frustration [69, 70].

The L phase is uniquely free of packing frustration, as its interfacial curvature and domain thicknesses are absolutely constant. Therefore, our discussion of packing frustration begins with the C phase. Figure 12 shows an end view of its cylindrical domains highlighting one of the Wigner–Seitz unit cells. The unit cell is then expanded showing the interface along with one representative diblock copolymer. On the left, we show a constant curvature interface, which minimizes the interfacial area but requires excessive stretching for those majority blocks oriented towards the six corners of the unit cell. On the right, the interface is adjusted so as to reduce this excessive stretching, but, in doing so, the interfacial area is increased. The competition between the tendencies for uniform curvature and uniform domain thickness will result in some intermediate interfacial shape.

In principal, the degree of packing frustration can be assessed by examining the variation in either curvature or domain thickness. However, since domain thickness is difficult to quantify in complicated morphologies, we will examine the former [58, 69]. Furthermore, sophisticated microscopy techniques are capable of directly measuring the interfacial curvature of even the G morphology [71]. Because of the periodicity of block copolymer morphologies, it is sufficient to consider the elementary interfacial units depicted in figure 13 for the C, G, PL and D morphologies. In each case, the variation in curvature H over the interface is indicated by a colour scale. We immediately see that C is virtually free of packing frustration compared to the three complex phases. To quantify the variation in curvature, we compute the standard deviations, σ_H. This demonstrates that, among the complex phases, G has the least packing frustration, which nicely accounts for its stability. Furthermore, the metastability of PL [9, 10] can be understood by the fact its packing frustration is only slightly higher. Naturally, the excessive frustration in D explains its complete absence from diblock copolymer melts [11]. Packing frustration also has an important effect on the classical C and S phases. Specifically, the hexagonal arrangement of cylinders and the bcc ordering of spheres are selected so as to minimize variations in the thickness of the majority domain [72].

We can associate packing frustration with the positions farthest from the interface, which can only be filled with highly stretched chains. For example, these positions in the C phase are the six corners of the Wigner–Seitz unit cell shown in figure 12. Not surprisingly, the free energy penalty due to packing frustration is somewhat less at lower segregations, where there is a naturally high interpenetration between the opposing brushes that form the domain [65]. This assertion is supported by the fact the relative variation in curvature, i.e. $\sigma_H/\langle H\rangle$, increases with segregation, χN [58]. As a consequence, the highly frustrated G phase becomes unstable

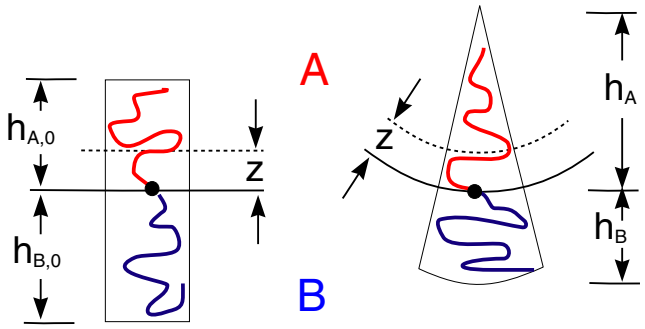

Figure 10. Diagram demonstrating the effect of interfacial curvature, H. For a flat interface, the area per chain remains invariant when moving away from the interface. However, for a curved interface, the area per chain changes by a factor $(1 - 2Hz)$, where z is the coordinate normal to the interface defined to be positive in the A domain and negative in the B domain. With this sign convention, positive curvature causes the height of the A brush, h_A, to increase relative to that of a flat interface, $h_{A,0}$, while h_B decreases relative to $h_{B,0}$.

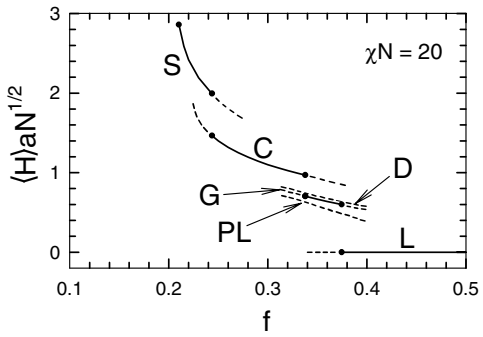

Figure 11. Area-averaged mean curvature, $\langle H \rangle$, as a function of diblock composition, f, calculated at $\chi N = 20$ using SCFT. The stable and metastable states are shown with solid and dashed curves, respectively, and the phase transitions are denoted by dots. As the diblock composition becomes asymmetric, the melt switches to structures with a higher interfacial curvature. Adapted from [69].

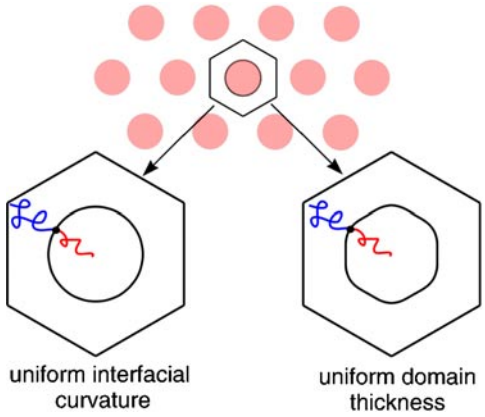

Figure 12. End view of the C phase showing the hexagonal arrangement of the minority cylinder domains along with one of the Wigner–Seitz unit cells, which is expanded below. The cell to the left has an interface of constant curvature, which minimizes the interfacial energy, while the cell on the right has a relatively uniform majority domain, which reduces its stretching energy.

relative to L and C phases beyond $\chi N \approx 60$ [12].

The minority domains of the complex phases, G, PL and D, are each constructed of struts connected together into lattices. The nodes of the lattice represent the points responsible for packing frustration within the minority domain. The D phase has the higher frustration because its nodes are four-fold coordinated as opposed to three-fold for G and PL [58]. Presumably, PL is less stable than G because of higher frustration in its majority domain. These hypotheses are easily tested using an idea of Gruner *et al* [70] for lyotropic liquid crystals. Packing frustration can be relieved in a given domain by adding the corresponding parent homopolymer, because it accumulates at the points responsible for frustration [73]. Consistent with this premise,

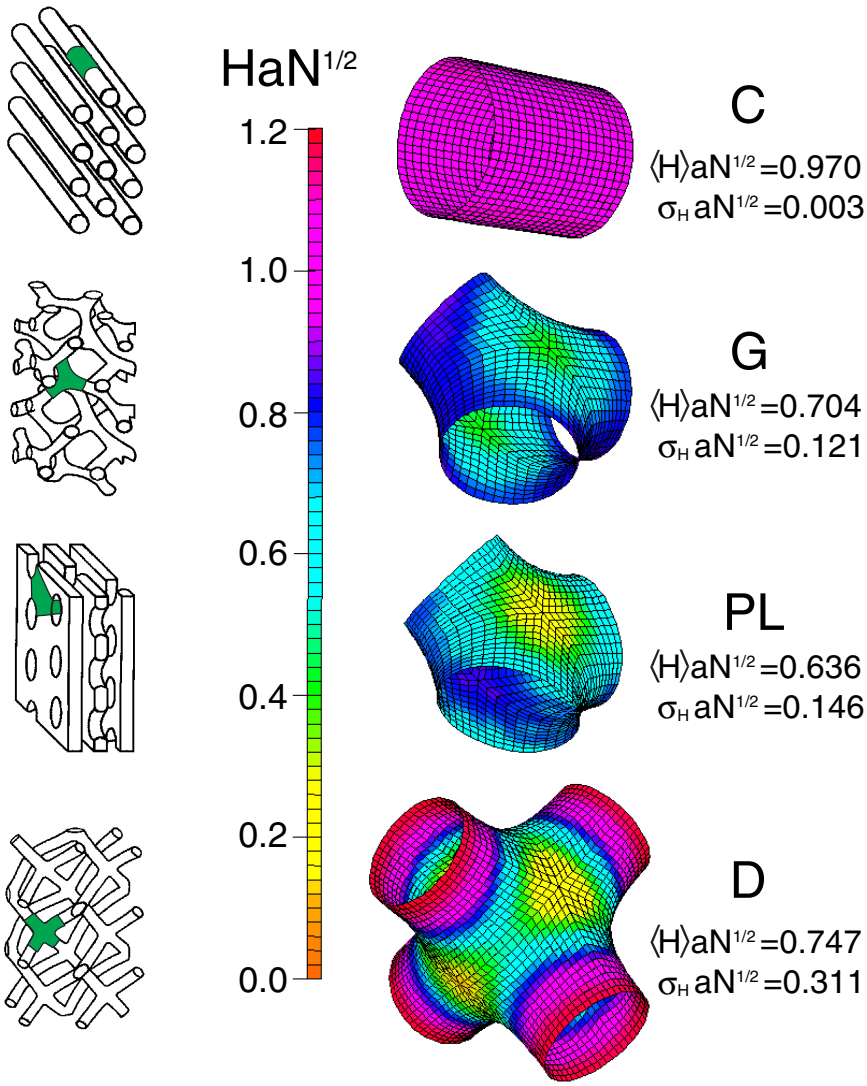

Figure 13. Interfacial curvature, H, distributions for the C, G, PL and D microstructures. The green patches on the schematic diagrams to the left indicate elementary interfacial units. The detailed shapes of these units are then displayed on the right by means of a SCFT calculation along the L/C phase boundary at $\chi N = 20$ and $f = 0.3378$. The curvature distribution over each unit is specified by the colour scale with the average and standard deviation quoted to the far right. Adapted from [69].

calculations [69] show that minority-type homopolymer reduces the packing frustration in D relative to G, whereas majority-type homopolymer does not. With PL, the converse is true. In fact, calculations [37, 73] predict that sufficient minority homopolymer can stabilise D over G, and that adequate majority homopolymer causes PL to replace G.

The presence of the close-packed spherical (S_{cp}) phase in figure 2(a) seems to contradict the idea that packing frustration favours the bcc arrangement. The explanation is that, at high asymmetries, a significant fraction of minority blocks are dislodged from their domains

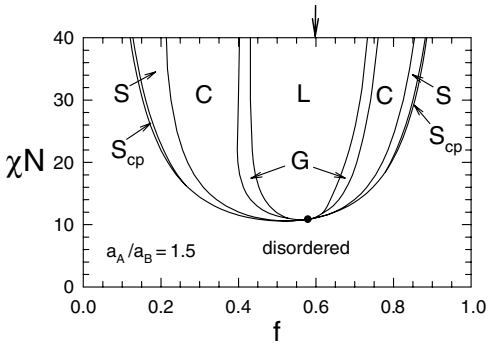

Figure 14. Theoretical phase diagram analogous to figure 2(a), but instead calculated for conformationally asymmetric diblock copolymers with $a_A/a_B = 1.5$. The vertical arrow indicates the composition where the interface of a strongly-segregated melt has zero spontaneous curvature. Adapted from [17].

by thermal fluctuations [58], producing *free* diblocks that swell the matrix and thus relieve packing frustration. This allows the spheres to switch to the close-packed arrangement as favoured by effective interactions between their coronas [75].

4.4. Conformational asymmetry

The theoretical phase diagram in figure 2 is symmetric about $f = 0.5$, whereas the experimental one possesses a slight asymmetry. This is partly attributed to the fact that the ratio of the polyisoprene and polystyrene statistical segment lengths is $a_{PI}/a_{PS} \approx 1.2$ [13], rather than one as assumed in the calculation. For other diblock copolymers where this ratio is much higher, the phase diagram is even more asymmetric [76]. Nevertheless, it is a trivial extension to include this asymmetry in the theory [17]; the resulting phase diagram for $a_A/a_B = 1.5$ is shown in figure 14. The main effect of the asymmetry is to shift the order–order transitions (OOTs) towards the right consistent with experiment [2, 76].

The shift in the OOTs is explained by the fact that segments with the longer statistical length are easier to stretch, and thus are favoured on the inside of interfacial curvature. The magnitude of the shift is easily estimated with a simple SST calculation. Generalizing equation (50) to include conformational asymmetry gives

$$F_{st} = F_{st,0}\left(1 - \frac{3HN}{2\Sigma\rho_0}\frac{(1-f)^2a_A^2 - f^2a_B^2}{(1-f)a_A^2 + fa_B^2}\right) \tag{51}$$

where the stretching energy of the flat interface is now

$$\frac{F_{st,0}}{nk_BT} = \frac{\pi^2N}{8\Sigma^2\rho_0^2}\left(\frac{f}{a_A^2} + \frac{1-f}{a_B^2}\right). \tag{52}$$

From equation (51), it follows that the point of zero spontaneous curvature shifts to $f = a_A/(a_A+a_B)$. This composition is indicated in figure 14 with an arrow and indeed corresponds well with the centre of the lamellar region.

5. Fluctuation effects

Although fluctuation effects in block copolymer melts are generally small, there are three instances where they significantly alter the mean-field predictions. A fruitful method of

handling these effects is to calculate the free energy in two steps; evaluate a Landau free energy for a fixed segment profile and then evaluate the partition function over all profiles. This effectively separates the problem into chain fluctuations and composition fluctuations.

To apply some rigour to this idea, we start with the exact free energy, F, expression,

$$\exp\left\{-\frac{F}{k_{\mathrm{B}}T}\right\} = \sum_{\{\boldsymbol{r}_\alpha(s)\}} \exp\left\{-\frac{\hat{H}}{k_{\mathrm{B}}T}\right\} \delta[\hat{\phi}_A(\boldsymbol{r}) + \hat{\phi}_B(\boldsymbol{r}) - 1] \tag{53}$$

where the sum is over all states of the system and the Hamiltonian,

$$\hat{H} = \hat{U} + \sum_{\alpha=1}^{n} \hat{E}_{st}[\boldsymbol{r}_\alpha(s); 0, 1] \tag{54}$$

combines the interaction energy (7) with the stretching energy (9). The delta functional selects out those configurations satisfying incompressibility (5). The Landau free energy, $F[\phi]$, expression,

$$\exp\left\{-\frac{F[\phi]}{k_{\mathrm{B}}T}\right\} = \sum_{\{\boldsymbol{r}_\alpha(s)\}} \exp\left\{-\frac{\hat{H}}{k_{\mathrm{B}}T}\right\} \delta[\hat{\phi}_A(\boldsymbol{r}) + \hat{\phi}_B(\boldsymbol{r}) - 1]\delta[\hat{\phi}_A(\boldsymbol{r}) - f - \phi(\boldsymbol{r})] \tag{55}$$

is very similar except that there is an additional delta functional that constrains the A segment profile to $\hat{\phi}_A(\boldsymbol{r}) = f + \phi(\boldsymbol{r})$. From the properties of the delta functional, it immediately follows that F is related to $F[\phi]$ by

$$\exp\left\{-\frac{F}{k_{\mathrm{B}}T}\right\} = \sum_{\phi(\boldsymbol{r})} \exp\left\{-\frac{F[\phi]}{k_{\mathrm{B}}T}\right\}. \tag{56}$$

Thus far, everything is exact, but the problem still remains untractable. To proceed, the typical approximation is to evaluate the Landau free energy $F[\phi]$ by mean-field theory. The Leibler free energy functional (29) is precisely that, assuming $\phi(\boldsymbol{r})$ remains small. For stronger segregations, $F[\phi]$ can be evaluated by SCFT [46,74] or alternatively by SST. The problem with mean-field theory is that it only constrains the ensemble-averaged concentration, $\phi_A(\boldsymbol{r})$, rather than the instantaneous concentration, $\hat{\phi}_A(\boldsymbol{r})$. Although this is a reasonable approximation at strong segregations where the fluctuations in $\hat{\phi}_A(\boldsymbol{r})$ are small, it is extremely questionable at the weak segregations where it is often applied.

5.1. Brazovskii fluctuations

In 1975, Brazovskii [77] calculated the phase behaviour for the class of Landau free energy functionals,

$$\frac{F[\phi]}{k_{\mathrm{B}}T} = \frac{1}{V}\int\left[\frac{\tau}{2}\phi^2(\boldsymbol{r}) + \frac{\xi_0^2}{8q^{*2}}\left[(\nabla^2 + q^{*2})\phi(\boldsymbol{r})\right]^2 - \frac{\gamma}{3!}\phi^3(\boldsymbol{r}) + \frac{\lambda}{4!}\phi^4(\boldsymbol{r})\right]\mathrm{d}\boldsymbol{r} \tag{57}$$

where τ, ξ, q^*, γ, and $\lambda > 0$ are free parameters. This class exhibits behaviour where the disordered phase (i.e. $\phi(\boldsymbol{r}) = 0$) becomes unstable to periodic modulations for wavevectors, $\boldsymbol{q}$, with $|\boldsymbol{q}| \approx q^*$ as τ switches from positive to negative, just as the block copolymer system does upon crossing the spinodal line. By mapping the Leibler free energy functional (29) onto the Brazovskii one, Fredrickson and Helfand [16] were able to extract fluctuation corrections for block copolymers. The original calculations only considered the L, C, and S ordered phases, but Podneks and Hamley have since extended the Brazovskii theory to include G [78] and then mapped the result onto the diblock copolymer system [79]. The Brazovskii fluctuations modify the phase behaviour near the mean-field critical point in figure 2(a) to that of figure 15. In short, the fluctuations destroy the weakly ordered structures shifting the ODT upwards.

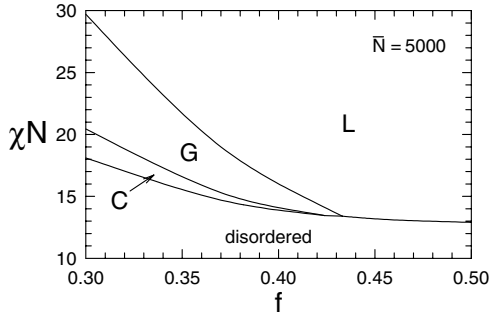

Figure 15. Fluctuation corrected phase diagram for diblock copolymer melts with an invariant polymerization index, $\bar{N} \equiv \rho_0^2 a^6 N = 5000$. Adapted from [79].

At $f = 0.5$, the ODT shifts to $\chi N = 10.495 + 41.022\bar{N}^{-1/3}$, where $\bar{N} \equiv \rho_0^2 a^6 N$ is the invariant polymerization index. This eliminates the critical point and generates direct first-order transitions between the ordered L, C and G phases and the disordered state in qualitative agreement with figure 2(b). Although there is good experimental evidence [80] supporting the Fredrickson–Helfand corrections, it is unrealistic to expect quantitative accuracy given their dependence on the mean-field Landau free energy functional (29).

5.2. Lattice melting

The close-packed spherical (S_{cp}) phase is affected by fluctuations in a more traditional way. Because of the relatively low energy required to pull the minority blocks from their spherical domains, the effective interaction binding the spheres together is unusually weak [58]. Based on experiment [81–83], the thermal fluctuations are sufficient to disrupt the periodic lattice in the same way fluctuations cause a conventional crystalline solid to melt into a liquid. The spherical micelles continue to exist but without any long-range order. Although it has been suggested [82] that the disordered micelles constitute their own phase, this is most certainly not the case; they instead become part of the disordered phase.

Dormidontova and Lodge [84] have proposed a fluctuation calculation for this effect. Although the results are in qualitative agreement with experiment, their calculation suffers from a common problem. The translational entropy of the spheres is calculated by counting the number of ways they can be distributed on a mesh. In this case, where the number of spherical domains is not conserved, the final predictions depend on the mesh size, which is unacceptable given that the mesh is an artificial construct. While this issue is well understood in other contexts (i.e. chemical reactions) [85], it is not fully appreciated by the soft condensed matter community. The consequence of this problem is revealed in the work by Kao and Olvera de la Cruz [86], where they are faced with three distinct expressions for the translational entropy of micelles. We are aware of one instance where Morse and Milner [87] have properly dealt with this issue in regards to membrane fluctuations. Ideally, a similar rigorous treatment should be applied to the diblock copolymer system.

5.3. Capillary waves

Experiments [88] have demonstrated that mean-field theory underestimates the interfacial width between the A and B domains. While the theory properly treats fluctuations where the junction of a single molecule deviates from the interface as shown in figure 16(a), it

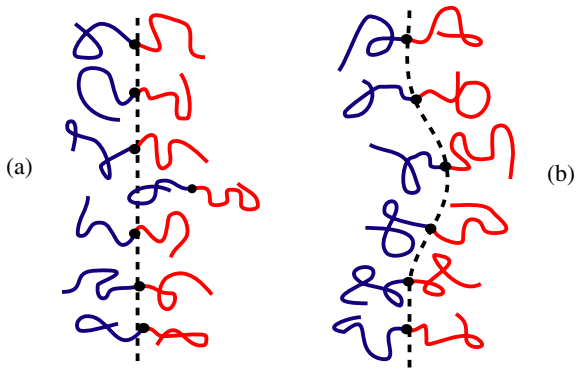

Figure 16. Thermal fluctuations involving (a) the motion of a single molecule versus (b) the cooperative motion of many molecules.

overestimates the energy for the collective motion depicted in figure 16(b). Consequently, mean-field theory suppresses *capillary waves* that are responsible for broadening the interface. The single-molecule motions are treated accurately because they only cause a small perturbation to the instantaneous fields, but the collective motions are not because they cause $\hat{w}_A(\boldsymbol{r})$ and $\hat{w}_B(\boldsymbol{r})$ to deviate significantly from their mean values, $w_A(\boldsymbol{r})$ and $w_B(\boldsymbol{r})$, respectively.

Nevertheless, it is, in principal, a simple matter to correct for capillary waves. Assuming a reasonable segregation, mean-field theory does produce an accurate Landau free energy for which there are no capillary waves due to the fact $\hat{\phi}_A(\boldsymbol{r})$ is constrained. Therefore, a capillary-wave corrected free energy, F, can be obtained by just summing the mean-field Landau free energy $F[\phi]$ over all profiles as prescribed in equation (56). Both Semenov [63] and Shull *et al* [89] have performed an approximate calculation of this nature for the L phase, predicting an interfacial width that nicely agrees with experiment [89, 90].

A more accurate treatment of capillary-wave fluctuations can be accomplished with the advanced method of Shi *et al* [46]. It also has the added benefit of providing the fluctuation-corrected scattering function for the ordered morphology. In fact, a major success of this method was the prediction of pretransitional fluctuations in the L phase at compositions close to the complex phase window [47], which experiments had incorrectly interpreted as a separate modulated-lamellar phase [8]. We now understand that a modulated-lamellar phase could not exist near the complex phase window, because it has the wrong interfacial curvature (i.e. $\langle H\rangle \approx 0$) plus it would be far too frustrated (i.e. large σ_H). Similar pretransitional fluctuations are evident near the C/S phase boundary [91], but unfortunately analogous calculations for nonlamellar phases are still only feasible at very weak segregations [41, 92].

6. Future work

In the last decade, the field of block copolymer phase behaviour has experienced significant advances, particularly in regards to the complex phases. It is now at a point where there is reasonable quantitative agreement between theory and experiment. Nevertheless, there remain several serious obstacles impeding our future progress.

6.1. Interaction parameter

Comparisons between experiment and theory rely on knowing the temperature-dependence of the Flory–Huggins χ parameter. It is generally assumed to obey the functional form,

$$\chi\rho_0 = \frac{\alpha}{T} + \beta \tag{58}$$

where α and β are constants[3]. We include the segment density ρ_0, because χ by itself is not an invariant quantity, a fact that is not always appreciated. The two terms are often labelled the enthalpic and entropic parts of χ, but we recommend that equation (58) is simply considered as a convenient functional fit. The fitting parameters, α and β, have been obtained by a wide range of theoretical–experimental comparisons [32]. In diblock copolymer melts, it is common to use either the ODT at $f = 0.5$ or the disordered-state scattering function. Since both of this quantities are affected by fluctuations, the comparisons are best performed with the Helfand–Fredrickson fluctuation corrected theory [16]. Alternatively, χ can extracted by analogous comparisons on binary homopolymer blends.

Ideally, diblock copolymer melts and binary blends would provide consistent values for α and β, but unfortunately they do not [32]. It is interesting to note that in some cases, such as the comparison of diblock and triblock ODTs [93], there is excellent consistency. Nevertheless, we cannot hope to conduct detailed experimental tests of the theory [94] until we can be confident of the χ parameter. Maurer *et al* [32] have argued that the inconsistencies stem from deficiencies in the current Helfand–Fredrickson fluctuation correction, and considering our above criticisms this a very reasonable suggestion. Still, there could be other contributing factors. Calculations have shown that chain stiffness has a significant effect on the diblock copolymer ODT [28], but not on the blend ODT [29]. Furthermore, we could expect that small nematic interactions would affect interfacial tension in block copolymer melts differently than in homopolymer blends, since in the former case the chains tend to be perpendicular to the interface [28] whereas in the latter case they tend to be parallel [29]. Hopefully, such issues are not important, and we can continue to use the simply Flory–Huggins interaction (27). If so, it may just be a matter of extracting χ based on more reliable theoretical predictions, such as domain sizes [95] or concentration profiles [90] of well-segregated melts.

6.2. Fluctuations

While the current Fredrickson–Helfand treatment has provided invaluable guidance regarding fluctuation effects, there is now a need for a quantitatively accurate theory. The weakness in the present approach is its reliance on the Leibler free energy functional (29). As stated above, mean-field theory cannot be expected to provide a reliable Landau free energy for weakly segregated melts, not to mention the fact the fourth-order expansion is insufficient to treat the segregations to which the ODT is typically shifted by fluctuation effects (see figure 15).

There are various possible ways to accurately incorporate fluctuation effects. One is to extend the existing SCFT, by going beyond the saddle-point approximation [5] used to approximate some of the difficult functional integrals. Stepanow [96] has attempted this by generating an expansion, where fluctuation corrections are represented by a series of graphs, much like in quantum field theory. Unfortunately, this approach has not been pushed to the point of producing useful predictions that can be tested against experiment. Naturally, Monte Carlo methods [97–99] and molecular dynamic simulations [100] constitute other viable

[3] For the PS–PI phase diagram in figure 2(b), the coefficients for the χ parameter in equation (58) are assumed to be $\alpha = 496$ K nm^{-3} and $\beta = -0.595$ nm^{-3} [13, 14].

approaches, although there are serious finite-size effects to contend with [101]. Also promising are new field-theoretic strategies [18] under investigation by Duechs and Schmid, where the functional integrals in SCFT are evaluated by Monte Carlo techniques, and by Ganesan and Fredrickson [102], where a complex Langevin method is employed.

6.3. Nonequilibrium

Future progress in the field of block copolymer phase behaviour will not only rely on further theoretical developments but also on the availability of accurate experimental data free of nonequilibrium artefacts. We should be aware that the phase boundaries in figure 2(b) are shifted by some unspecified amount due to the finite heating rate ($\sim 1\,^{\circ}\mathrm{C\ min}^{-1}$) applied during the experiment. In fact, the finite rate was responsible for misinterpreting PL as a stable phase, an assertion that contradicted theory for several years [9, 12].

When working with large polymeric molecules, the progression towards equilibrium can often be very slow. This fact has been clearly demonstrated by a simple but very enlightening experiment by Lipic *et al* [103], where identical samples were prepared by two different routes and annealed at 40 °C above the glass transition for prolonged periods by current standards (up to 4 weeks). In numerous cases, the two different routes resulted in totally distinct morphologies, and even when the morphologies were the same the domain spacings differed by upto 17%. This is particularly shocking given that the experiment was performed at rather modest segregations, $\chi N \approx 40$.

Clearly, there is further need to investigate block copolymer kinetics. Considerable work is now proceeding on the kinetics of order–order [91,104,105] and order–disorder [81] transitions, and some measurements have examined single-chain diffusion in a lamellar morphology [106]. However, a general appreciation for the time required by block copolymer systems to respond to a perturbation such as a temperature jump is still lacking. Even straightforward experiments, such as monitoring the response of the domain spacing as a function of segregation, have yet to be performed.

7. Summary

Our fundamental understanding of block copolymer systems has matured substantially over recent years due to the strong interplay between experiment and theory. The theoretical successes can be largely attributed to the standard Gaussian model and the fact that thermal fluctuations are small. In particular, the individual molecules of the melt can be accurately represented by elastic threads interacting via simple contact forces, and the statistical mechanics of this microscopic coarse-grained model can be reliably evaluated under the mean-field approximation. Furthermore, important mathematical conveniences permit exact numerical mean-field calculations for arbitrarily complex periodic morphologies as well as analytic expressions for both weakly and strongly segregated melts.

Theory has provided a nice simple understanding of the ordered morphologies in terms of their internal interfacial energy and the entropic penalty of stretching polymer molecules. First of all, the domain size, or equivalently area per molecule, is selected so as to balance these two free energy contributions. Secondly, the interface acquires a preferred, or rather spontaneous, curvature in order to balance the stretching energy between the A and B blocks. It is this mechanism that causes the order–order phase transitions. Thirdly, the interfaces adjust their detailed shape so as to simultaneously produce uniform curvature to minimize interfacial energy and uniform domains to minimize stretching energy. An inability to do so, referred to as packing frustration, is responsible for excluding various morphologies, such as PL and D, from the equilibrium phase diagrams in figure 2.

Although mean-field theory is generally valid for block copolymer melts, there are several instances in which fluctuation effects are important. Firstly, Brazovskii fluctuations destroy the weakly ordered morphologies near the mean-field critical point in figure 2(a), shifting the ODT upwards and causing direct transitions from the L, G, and C ordered phases to the disordered state. Secondly, in the spherical phase near the ODT, fluctuations prevent the minority domains from forming an ordered lattice, thus transforming the mean-field S_{cp} phase into part of the disordered state. Thirdly, there are significant interfacial fluctuations, although their only known consequence is to broaden the effective width of the interface and to produce pretransitional effects in SAXS patterns and rheology scans.

Further quantitative improvement between theory and experiment will depend on resolving several challenging problems. First of all, it will be necessary to establish whether or not the simple Flory–Huggins interaction (7) is adequate, and if so determine a reliable technique for accurately extracting the temperature dependence of χ. Secondly, an improved method of treating fluctuations is needed. Thirdly, experiments will have to cope more carefully with nonequilibrium effects in order to provide reliable benchmarks for testing new theoretical predictions. Naturally, basic research of this nature will enhance the role of block copolymers as a model system for studying the wide range of phenomena associated with complex molecular self-assembly, as well as benefiting those engaged in block copolymer applications.

Acknowledgments

This review has benefited from many valuable interactions with people such as Frank Bates, Damian Hajduk, Marc Hillmyer, Tim Lodge, Dave Morse, Tony Ryan, Michael Schick, Friederike Schmid and Mark Whitmore. I am particularly indebted to An-Chang Shi for introducing me to SCFT and suggesting a Fourier-space approach, which has proven to be so powerful. This work was supported by the EPSRC (GR/M61160).

References

[1] Seddon J M 1990 *Biochim. Biophys. Acta* **1031** 1
Seddon J M and Templer R H 1993 *Phil. Trans. R. Soc.* A **344** 377
Seddon J M and Templer R H 1995 *Handbook of Biological Physics* vol 1, ed A J Hoff (Amsterdam: Elsevier)
[2] Bates F S and Fredrickson G H 1999 *Phys. Today* **52** 32
[3] Helfand E 1975 *J. Chem. Phys.* **62** 999
[4] Helfand E 1975 *Macromolecules* **8** 552
[5] Matsen M W and Schick M 1994 *Phys. Rev. Lett.* **72** 2660
[6] Hajduk D A, Harper P E, Gruner S M, Honeker C C, Kim G, Thomas E L and Fetters L J 1994 *Macromolecules* **27** 4063
[7] Schulz M F, Bates F S, Almdal K and Mortensen K 1994 *Phys. Rev. Lett.* **73** 86
[8] Hamley I W, Koppi K A, Rosedale J H, Bates F S, Almdal K and Mortensen K 1993 *Macromolecules* **26** 5959
Hamley I W, Gehlsen M D, Khandpur A K, Koppi K A, Rosedale J H, Schulz M F, Bates F S, Almdal K and Mortensen K 1994 *J. Phys. II (France)* **4** 2161
[9] Hajduk D A, Takenouchi H, Hillmyer M A, Bates F S, Vigild M E and Almdal K 1997 *Macromolecules* **30** 3788
[10] Vigild M E, Almdal K, Mortensen K, Hamley I W, Fairclough J P A and Ryan A J 1998 *Macromolecules* **31** 5702
[11] Hajduk D A, Harper P E, Gruner S M, Honeker C C, Kim G, Thomas E L and Fetters L J 1995 *Macromolecules* **28** 2570
[12] Matsen M W and Bates F S 1996 *Macromolecules* **29** 1091
[13] Bates F S, Schulz M F, Khandpur A K, Förster S, Rosedale J H, Almdal K and Mortensen K 1994 *Faraday Discuss.* **98** 7
[14] Förster S, Khandpur A K, Zhao J, Bates F S, Hamley I W, Ryan A J and Bras W 1994 *Macromolecules* **27** 6922
[15] Khandpur A K, Förster S, Bates F S, Hamley I W, Ryan A J, Bras W, Almdal K and Mortensen K 1995 *Macromolecules* **28** 8796

[16] Fredrickson G H and Helfand E 1987 *J. Chem. Phys.* **87** 697
[17] Matsen M W and Bates F S 1997 *J. Polym. Sci.* B **35** 945
[18] Fredrickson G H, Ganesan V and Drolet F *Macromolecules* at press
[19] Schmid F 1998 *J. Phys.: Condens. Matter* **10** 8105
[20] Whitmore M D and Vavasour J D 1995 *Acta. Polymerica* **46** 341
[21] Bates F S and Fredrickson G H 1990 *Ann. Rev. Phys. Chem.* **41** 512
[22] Fredrickson G H and Bates F S 1996 *Ann. Rev. Mater. Sci.* **26** 501
[23] Hamley I W 1998 *The Physics of Block Copolymers* (Oxford: Oxford University Press)
[24] Jones R A L and Richards R W 1999 *Polymers at Surfaces and Interfaces* (Cambridge: Cambridge University Press)
[25] Goodman I 1982 *Developments in Block Copolymers* (New York: Applied Science)
[26] Hajduk D A, Gruner S M, Erramilli S, Register R A and Fetters L J 1996 *Macromolecules* **29** 1473
[27] Netz R R and Schick M 1996 *Phys. Rev. Lett.* **77** 302
[28] Matsen M W 1996 *J. Chem. Phys.* **104** 7758
[29] Morse D C and Fredrickson G H 1994 *Phys. Rev. Lett.* **73** 3235
[30] Takahashi K and Yunoki Y 1967 *J. Phys. Soc. Japan* **22** 219
[31] Doi M and Edwards S F 1986 *The Theory of Polymer Dynamics* (Oxford: Oxford University Press)
[32] Maurer W W, Bates F S, Lodge T P, Almdal K, Mortensen K and Fredrickson G H 1998 *J. Chem. Phys.* **108** 2989
[33] Matsen M W and Thompson R B 1999 *J. Chem. Phys.* **111** 7139
Matsen M W 2000 *J. Chem. Phys.* **113** 5539
[34] Kavassalis T A and Whitmore M D 1991 *Macromolecules* **24** 5430
Matsen M W and Schick M 1994 *Macromolecules* **27** 7157
[35] Matsen M W and Schick M 1994 *Macromolecules* **27** 6761
[36] Matsen M W 1998 *J. Chem. Phys.* **108** 785
[37] Matsen M W 1995 *Phys. Rev. Lett.* **74** 4225
[38] Hong K M and Noolandi J 1981 *Macromolecules* **14** 727
[39] Spontak R J *et al* 1996 *Macromolecules* **29** 4494
[40] Matsen M W and Bates F S 1995 *Macromolecules* **28** 7298
[41] Laradji M, Shi A-C, Noolandi J and Desai R C 1997 *Macromolecules* **30** 3242
[42] Drolet F and Fredrickson G H 1999 *Phys. Rev. Lett.* **83** 4317
[43] Leibler L 1980 *Macromolecules* **13** 1602
[44] Marques C M and Cates M E 1990 *Europhys. Lett.* **13** 267
[45] Milner S T and Olmsted P D 1997 *J. Phys. II (France)* **7** 249
[46] Shi A-C, Noolandi J and Desai R C 1996 *Macromolecules* **29** 6487
[47] Yeung C, Shi A-C, Noolandi J and Desai R C 1996 *Macromol. Theory Simul.* **5** 291
[48] Semenov A N 1985 *Sov. Phys.–JETP* **61** 733
[49] Broseta D, Fredrickson G H, Helfand E and Leibler L 1990 *Macromolecules* **23** 132
[50] Milner S T, Witten T A and Cates M E 1988 *Europhys. Lett.* **5** 413
[51] Goldstein H 1980 *Classical Mechanics* 2nd edn (Philippines: Addison-Wesley)
[52] Pereira G G 2001 *Phys. Rev.* E **63** 061809
Matsen M W *Phys. Rev.* E submitted
[53] Likhtman A E and Semenov A N 1997 *Macromolecules* **30** 7273
[54] Olmsted P D and Milner S T 1998 *Macromolecules* **31** 4011
[55] Fredrickson G H 1991 *Macromolecules* **24** 3456
[56] Olmsted P D and Milner S T 1994 *Phys. Rev. Lett.* **72** 936
Olmsted P D and Milner S T 1995 *Phys. Rev. Lett.* **74** 829
[57] Likhtman A E and Semenov A N 1994 *Macromolecules* **27** 3103
[58] Matsen M W and Bates F S 1996 *J. Chem. Phys.* **106** 2436
[59] Hajduk D A, Gruner S M, Rangarajan P, Register R A, Fetters L J, Honeker C, Albalak R J and Thomas E L 1994 *Macromolecules* **27** 490
[60] Matsen M W and Whitmore M D 1996 *J. Chem. Phys.* **105** 9698
[61] Ball R C, Marko J F, Milner S T and Witten T A 1994 *Macromolecules* **24** 693
[62] Matsen M W 2001 *J. Chem. Phys.* **114** 10 528
[63] Semenov A N 1993 *Macromolecules* **26** 6617
[64] Matsen M W and Gardiner J M 2000 *J. Chem. Phys.* **113** 1673
[65] Matsen M W and Bates F S 1995 *Macromolecules* **28** 8884
[66] Goveas J L, Milner S T and Russel W B 1997 *Macromolecules* **30** 5541

[67] Likhtman A E and Semenov A N 2000 *Europhys. Lett.* **51** 307
[68] Thomas E L, Anderson D M, Henkee C S and Hoffman D 1988 *Nature* **334** 598
[69] Matsen M W and Bates F S 1996 *Macromolecules* **29** 7641
[70] Gruner S M 1989 *J. Phys. Chem.* **93** 7562
[71] Jinnai H, Nishikawa Y, Spontak R J, Smith S D, Agard D A and Hashimoto T 2000 *Phys. Rev. Lett.* **84** 518
Jinnai H, Kajihara T, Watashiba H, Nishikawa Y and Spontak R J 2001 *Phys. Rev.* E **64** 010803
[72] Thomas E L, Kinning D J, Alward D B and Henkee C S 1987 *Macromolecules* **20** 2934
[73] Matsen M W 1995 *Macromolecules* **28** 5765
[74] Matsen M W 1998 *Phys. Rev. Lett.* **80** 4470
[75] Semenov A N 1989 *Macromolecules* **22** 2849
[76] Mai S M, Fairclough J P A, Terrill N J, Turner S C, Hamley I W, Matsen M W, Ryan A J and Booth C 1998 *Macromolecules* **31** 8110
[77] Brazovskii S A 1975 *Sov. Phys.–JETP* **41** 85
[78] Podneks V E and Hamley I W 1996 *JETP Lett.* **41** 617
[79] Hamley I W and Podneks V E 1997 *Macromolecules* **30** 3701
[80] Bates F S, Rosedale J H, Fredrickson G H and Glinka C J 1988 *Phys. Rev. Lett.* **61** 2229
Bates F S, Rosedale J H and Fredrickson G H 1990 *J. Chem. Phys.* **92** 6255
[81] Sakamoto N and Hashimoto T 1998 *Macromolecules* **31** 8493
[82] Sakamoto N, Hashimoto T, Han C D, Kim D and Vaidya N Y 1997 *Macromolecules* **30** 1621
[83] Han C D, Vaidya N Y, Kim D, Shin G, Yamaguchi D and Hashimoto T 2000 *Macromolecules* **33** 3767
[84] Dormidontova E E and Lodge T P *Macromolecules* **34** 9143
[85] Reif K 1965 *Fundamentals of Statistical and Thermal Physics* (New York: McGraw-Hill)
[86] Kao C R and Olvera de la Cruz M 1990 *J. Chem. Phys.* **93** 8284
[87] Morse D C and Milner S T 1995 *Phys. Rev.* E **52** 5918
[88] Anastasiadis S H, Russell T P, Satija S K and Majkrzak C F 1990 *J. Chem. Phys.* **92** 5677
[89] Shull K R, Mayes A M and Russell T P 1993 *Macromolecules* **26** 3929
[90] Koneripalli N, Levicky R, Bates F S, Matsen M W, Satija S, Ankner J and Kaiser H 1998 *Macromolecules* **31** 3498
[91] Ryu C Y, Vigild M E and Lodge T P 1998 *Phys. Rev. Lett.* **81** 5354
Ryu C Y and Lodge T P 1999 *Macromolecules* **32** 7190
[92] Laradji M, Shi A-C, Desai R C and Noolandi J 1997 *Phys. Rev. Lett.* **78** 2577
Matsen M W 1998 *Phys. Rev. Lett.* **80** 201
[93] Mai S M, Mingvanish W, Turner S C, Chaibundit C, Fairclough J P A, Heatley F, Matsen M W, Ryan A J and Booth C 2000 *Macromolecules* **33** 5124
[94] Lai C, Russel W B, Register R A, Marchand G R and Adamson D H 2000 *Macromolecules* **33** 3461
[95] Ren Y, Lodge T P and Hillmyer M A 2000 *Macromolecules* **33** 866
[96] Stepanow S 1995 *Macromolecules* **28** 8233
[97] Hoffmann A, Sommer J U and Blumen A 1997 *J. Chem. Phys.* **107** 7559
[98] Besold G, Hassager O and Mouritsen O G 1999 *Comput. Phys. Commun.* **122** 542
[99] Fried H and Binder K 1991 *J. Chem. Phys.* **94** 8349
Fried H and Binder K 1993 *Macromolecules* **26** 6878
[100] Murat M, Grest G S and Kremer K 1999 *Macromolecules* **32** 595
[101] Micka U and Binder K 1995 *Macromol. Theor. Simul.* **4** 419
[102] Ganesan V and Fredrickson G H 2001 *Europhys. Lett.* **55** 814
[103] Lipic P M, Bates F S and Matsen M W 1999 *J. Polym. Sci.* B **37** 2229
[104] Hajduk D A, Ho R M, Hillmyer M A, Bates F S and Almdal K 1998 *J. Chem. Phys.* **102** 1356
[105] Floudas G, Ulrich R, Wiesner U and Chu B 2000 *Europhys. Lett.* **50** 182
Floudas G, Ulrich R and Wiesner U 1999 *J. Chem. Phys.* **110** 652
[106] Lodge T P and Dalvi M C 1995 *Phys. Rev. Lett.* **75** 657